Band gaps and cavity modes in dual phononic and photonic strip waveguides

Yan Pennec, Bahram Djafari-Rouhani, C. Li, J.M. Escalante, Alejandro Martínez, Sarah Benchabane, Vincent Laude, Nikos Papanikolaou

Band gaps and cavity modes in dual phononic and photonic strip waveguides

Y. Pennec, B. Djafari Rouhani, C. Li, J. M. Escalante, A. Martinez et al.

Citation: AIP Advances **1**, 041901 (2011); doi: 10.1063/1.3675799

View online: http://dx.doi.org/10.1063/1.3675799

View Table of Contents: http://aipadvances.aip.org/resource/1/AAIDBI/v1/i4

Published by the American Institute of Physics.

Band gaps and cavity modes in dual phononic and photonic strip waveguides

Y. Pennec,[1] B. Djafari Rouhani,[1] C. Li,[1] J. M. Escalante,[2] A. Martinez,[2] S. Benchabane,[3] V. Laude,[3] and N. Papanikolaou[4]
[1]*Institut d'Electronique, Microélectronique et Nanotechnologie, UMR CNRS 8520 Université Lille 1, Villeneuve d'Ascq, France*
[2]*Nanophotonics Technology Center, Universidad Politécnica de Valencia, Spain*
[3]*Institut FEMTO-ST, Université de Franche Comté and CNRS, Besançon, France*
[4]*Institute of Microelectronic, NCSR, Athena, Greece*

(Received 10 October 2011; accepted 2 December 2011; published online 23 December 2011)

We discuss theoretically the simultaneous existence of phoxonic, i.e., dual phononic and photonic, band gaps in a periodic silicon strip waveguide. The unit-cell of this one-dimensional waveguide contains a hole in the middle and two symmetric stubs on the sides. Indeed, stubs and holes are respectively favorable for creating a phononic and a photonic band gap. Appropriate geometrical parameters allow us to obtain a complete phononic gap together with a photonic gap of a given polarization and symmetry. The insertion of a cavity inside the perfect structure provides simultaneous confinement of acoustic and optical waves suitable to enhance the phonon-photon interaction. *Copyright 2011 Author(s). This article is distributed under a Creative Commons Attribution 3.0 Unported License*. [doi:10.1063/1.3675799]

I. INTRODUCTION

Phononic[1,2] and photonic crystals[3,4] have both received a great deal of attention during the last two decades. These infinite 2D periodic structures, constituted by a periodical repetition of inclusions in a matrix background, have opened up new avenues for controlling sound and light, leading to the proposition of many novel acoustic[5] and optical[6] devices. The interest on these structures is partly based on their ability to exhibit absolute band gaps and localized modes associated with defects forming waveguides and cavities. The existence of band gaps and confined modes has especially been investigated in photonic crystal slabs[7,8] and more recently in phononic crystal slabs,[9–13] in particular in view of the technological realization of integrated structures for electronics and telecommunications. A related structure, widely used in photonics, is constituted by a 1D narrow strip waveguide, for instance a silicon waveguide, periodically drilled with holes. Such 1D photonic crystals are recognized for their ability to manipulate light and are promising as interconnects for the integration of optical functions on a chip.[14–16] However, few studies have dealt with the phononic properties of periodic strip waveguides.[17]

Following recent advances in nanotechnology fabrication, the simultaneous control of phonons and photons in the same structure, with the aim of enhancing their interaction, has received a great deal of attention during the last few years. Dual phononic-photonic (also called phoxonic) structures hold promises for the simultaneous confinement and tailoring of sound and light waves, with potential applications to acousto-optical devices and highly controllable phonon-photon interactions. The existence of dual photonic and phononic band gaps has been investigated first in 2D infinite crystals of air holes drilled in silicon,[18,19] lithium niobate,[20] or sapphire matrices.[21] Similar demonstrations have been performed in 2.5D silicon crystal slabs with inclusions composed of holes,[22,23] pillars,[24] or "snow-flake" structures.[25] The periodic slab is also used to design linear[25–27] and cavity defects[28,29] in which the confinement of both excitations or the existence of slow waves is expected to strongly enhance their interaction.

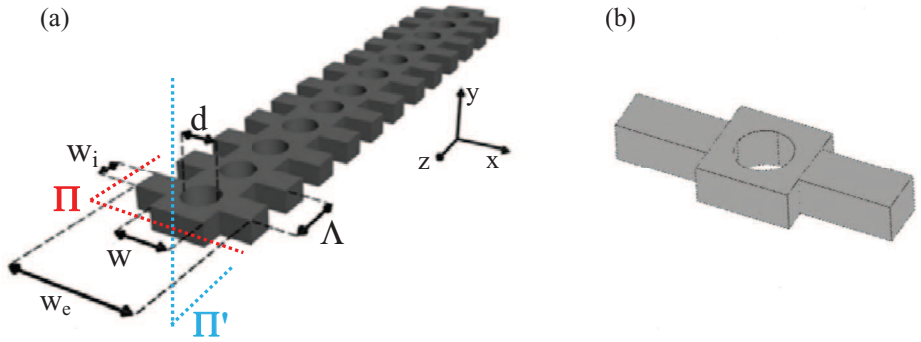

FIG. 1. (a) Schematic view of the periodic silicon strip waveguide. (b) Representation of the unit cell which contains one hole in the middle of the waveguide and two symmetric stubs on each side.

The enhancement of photon-phonon interaction has been also investigated in 1D strip waveguides. Eichenfield *et al.*[30,31] proposed a 1D patterned optomechanical nanobeam made up of a periodic array of rectangular shaped holes in a straight waveguide. Optically, the structure has a complete photonic band gap, but not a mechanical gap. This makes the structure susceptible of mechanical losses, especially when a cavity is inserted. It remains that, up to now, the theoretical demonstration of a complete absolute phononic and photonic band gap in 1D nanobeam structure is still missing.

The aim of this paper is to investigate both the acoustic and optical band structures, and in particular the existence of dual phononic-photonic band gaps, in a model silicon strip waveguide in which each unit cell contains one hole in the middle and two symmetric stubs on the sides. The geometry of the structure is motivated by stubs and holes being favorable for the opening of phononic and photonic gaps, respectively. In section II, we present the methods of calculations we have used, namely the finite-element (FE) method for dispersion curves and the finite difference time domain (FDTD) method for transmission spectra. In section III, we discuss the existence and evolution of band gaps as a function of the geometrical parameters of the structure. Then, we show in section IV the simultaneous confinement of phonons and photons when a defect cavity is inserted inside the strip waveguide. Conclusions are presented in section V.

II. MODEL AND METHOD OF CALCULATION

Figure 1(a) depicts the periodical silicon strip waveguide made up of a straight waveguide combined with symmetric stubs grafted on each side and circular holes drilled in the middle. The choice of silicon is motivated both by its technological interest in electronics and telecommunications and the fact that silicon strips are able to guide optical waves. Silicon is taken as a cubic material with elastic constants C_{11}=165.7 GPa, C_{12}=63.9 GPa, C_{44}=79.62 GPa, and mass density ρ=2331 kg/m^3. Silicon is optically isotropic with a refractive index of 3.47. In Figure 1(a), the z axis is directed along the strip waveguide and defines the propagation direction. The y axis is chosen perpendicular to the strip waveguide and parallel to the axis of the hole. The lattice period Λ can be considered as the unit of length. Then, the geometrical parameters involved in the structure are the width of the waveguide w=Λ, the length w_e and width w_i of the symmetric stubs, the thickness h of the strip and the diameter d=2r of the air hole. Figure 1(b) shows the elementary unit cell. Bloch-Floquet periodic boundary conditions are applied on the sides of the unit cell that are orthogonal to the z axis. In phononic calculations, stress-free boundary conditions are applied on all other surfaces of the strip, since elastic waves cannot propagate in air. In photonic calculations, one has to consider a large volume of air around the strip and artificial periodic boundary conditions are applied in the x and y directions. The air thickness in each direction is taken as five times the lattice parameter Λ, in order to ensure convergence of the dispersion diagram under the light cone. The guided photonic modes and their associated band gaps are specifically searched for under the light cone, since above

the light line modes can radiate in air. Due to small imperfections occurring during the fabrication of actual samples, the guided modes may couple to leaky waves above the light line and thus become lossy. Such radiation losses are, however, not considered in our calculations. The structure shown in Fig. 1(a) possesses two symmetry planes, Π (normal to y) and Π' (normal to x), so that all branches in the dispersion curves can be labeled according to their symmetry (odd or even) with respect to these planes.

In all band diagrams presented in this paper, frequencies are given in the dimensionless units $\Omega=\omega\Lambda/2\pi c$, where c is either the velocity of light in vacuum for electromagnetic waves or the transverse velocity of sound in silicon (c_t=5844m/s) for elastic waves.

III. PHONONIC/PHOTONIC BAND GAPS

The purpose of this section is to find dual phononic and photonic band gaps in the structured nanobeam of Fig. 1. Up to now, strip waveguides have been mainly studied in photonics where the possibility of band gaps was demonstrated both in straight waveguides containing air holes[14] and in stubbed waveguides.[16] Regarding elastic waves, Hsu *et al.*[17] discussed the formation of phononic band gaps in strip waveguides cut from a phononic crystal plate. Eichenfield *et al.*[30,31] studied an optomechanical straight nanowire containing periodic rectangular holes supporting photonic band gaps but no phononic band gaps. The demonstration of dual phononic-photonic gaps in strip waveguides is therefore still missing and is the subject of the following investigation. The insertion of periodical holes in the waveguide is actually sufficient to create a photonic band gap while the stubbed waveguide supports phononic band gaps. For this reason, we propose to study the geometry of Fig. 1 where each unit cell contains a combination of a hole and two symmetric stubs. By varying the geometrical parameters, we shall show that the phononic band gap is mainly sensitive to the size of the stubs whereas it is practically independent of the diameter of the hole. On the other hand, the diameter of the hole plays the most significant role in the photonic dispersion curves.

Figure 2(a) displays the phononic dispersion diagram in the first Brillouin zone, for geometrical parameters w_e/Λ=3.0, w_i/Λ=0.5, h/Λ=0.44, and r/Λ=0.3. As expected, the band diagram of the nanobeam shows four acoustic branches starting from the Γ point. At higher frequencies, a complete phononic band gap is found in the reduced frequency range [0.306, 0.355]. In Figs. 2(b) to 2(e), we show the evolution of this gap as a function of the geometrical parameters of the structure.

Figure 2(b) represents the band gap map for a variation of the full length w_e/Λ of the symmetric stubs. The gap is opened in a large range of values of w_e, from 2.7Λ to 3.7Λ, with a decrease in the central frequency of the gap as w_e increases. In Fig. 2(c), one can see that in order to open the gap, the width of the stubs has to be larger than 0.3Λ. For a width $w_i \geq 0.5\Lambda$, the width and frequency of the gap remain almost constant. These trends support the fact that the geometrical parameters of the stub affect very significantly the formation of the phononic gap. The evolution of the band gaps as a function of the thickness of the strip is sketched in figure 2(d). As in the case of a phononic slab drilled with holes,[9] the thickness has to be close to half the lattice parameter. Finally, the band gap is not very sensitive to the radius of the holes (Fig. 2(e)) and remains open for any radius ranging from 0 to 0.45Λ.

Keeping the geometrical parameters of the stubs suitable for the opening of a phononic band gap (w_i/Λ=0.5 and w_e/Λ=3.0) and choosing a thickness h/Λ=0.44, we study in Fig. 3 the variations of the photonic dispersion diagram as a function of the radius of the hole. Band diagrams are presented for r/Λ=0.0, 0.3, and 0.45. By increasing the radius of the hole from zero, the branches under the light cone, which represent guided modes of the strip, move upwards. Therefore, the number of branches decreases in a large frequency range corresponding to Λ/λ smaller than 0.35. Although there is no absolute photonic band gap for an arbitrary polarization of light, one can search for band gaps for modes which are of a given symmetry with respect to the symmetry planes Π' and Π of the structure (see Fig.1).

A symmetry analysis can been conducted from the calculation of the electric and magnetic fields associated with the branches in Fig. 3(b). For the lowest four branches, this assignment is supported by the field maps in Fig. 4 of the x component of the electric field at the reduced wavenumber $k\Lambda/2\pi$=0.414. The first and third branches have the same symmetry oe, namely odd with respect

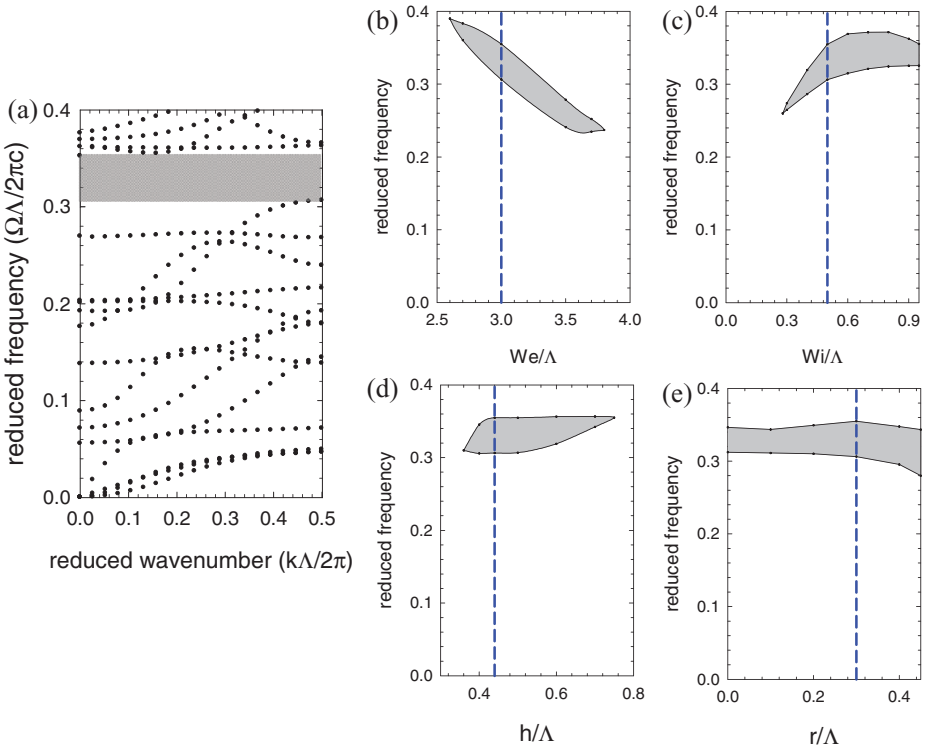

FIG. 2. (a) Phononic dispersion diagram for the stubbed waveguide of figure 1 with parameters $w_e/\Lambda=3.0$, $w_i/\Lambda=0.5$, $h/\Lambda=0.44$, and $r/\Lambda=0.3$. (b, c, d and e) Evolution of band gap edges as a function of each geometrical parameter, the others being kept constant: (b) w_e/Λ, (c) w_i/Λ, (d) h/Λ and (e) r/Λ. The vertical blue dashed lines give the values of the parameters used in the calculation of the dispersion diagram presented in (a).

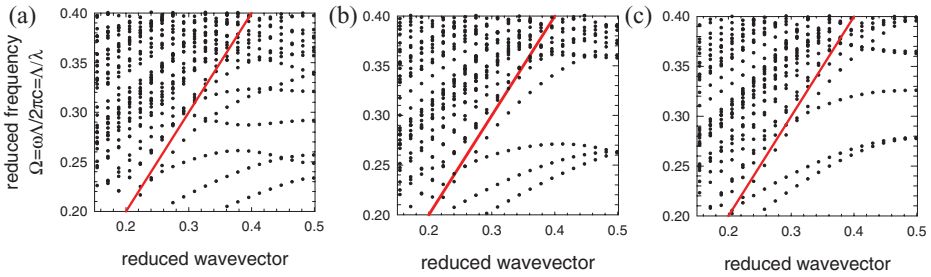

FIG. 3. Photonic dispersion diagrams for the same parameters ($h/\Lambda=0.44$, $w_i/\Lambda=0.5$ and $w_e/\Lambda=3.0$) as in figure 2(a), but for three different radii: (a) $r/\Lambda=0.0$, (b) $r/\Lambda=0.3$ and (c) $r/\Lambda=0.45$. In figure (b), modes are labeled as odd (o) or even (e) with respect to the symmetry planes Π' and Π of the structure. The reduced frequency is given by $\Omega=\omega\Lambda/2\pi c=\Lambda/\lambda$, where c is the velocity of light in vacuum.

to Π' and even with respect to Π. The second and fourth branches are respectively ee and eo. Therefore, there is a wide photonic gap with oe symmetry in the frequency range [0.270, 0.337] between branches 1 and 3. Incident light with such symmetry can only excite the latter branches and therefore cannot propagate in the range of the frequency range of the gap.

IV. PHONONIC/PHOTONIC CAVITY MODE

The strip waveguide defined in the previous section with geometrical parameters $w_e/\Lambda=3.0$, $w_i/\Lambda=0.5$, $h/\Lambda=0.44$, and $r/\Lambda=0.3$, presents a full phononic band gap and a photonic band gap of a given symmetry. The aim of this section is to show the possibility of simultaneous confinement of

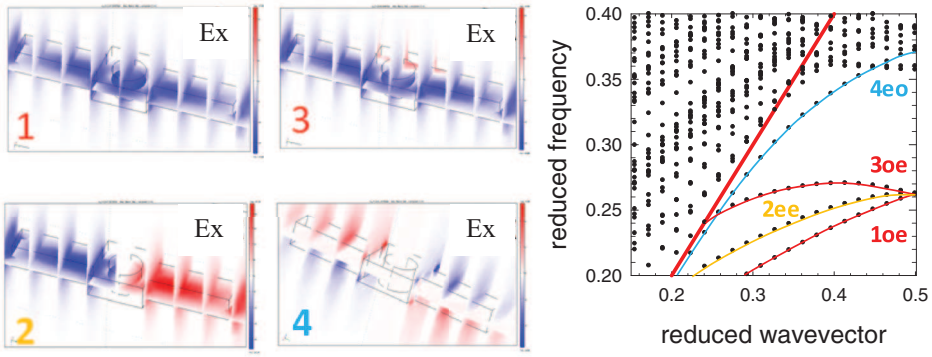

FIG. 4. Map of the x component of the electric field for the lowest four modes in Fig. 3(b) at the reduced wavenumber $k\Lambda/2\pi=0.414$.

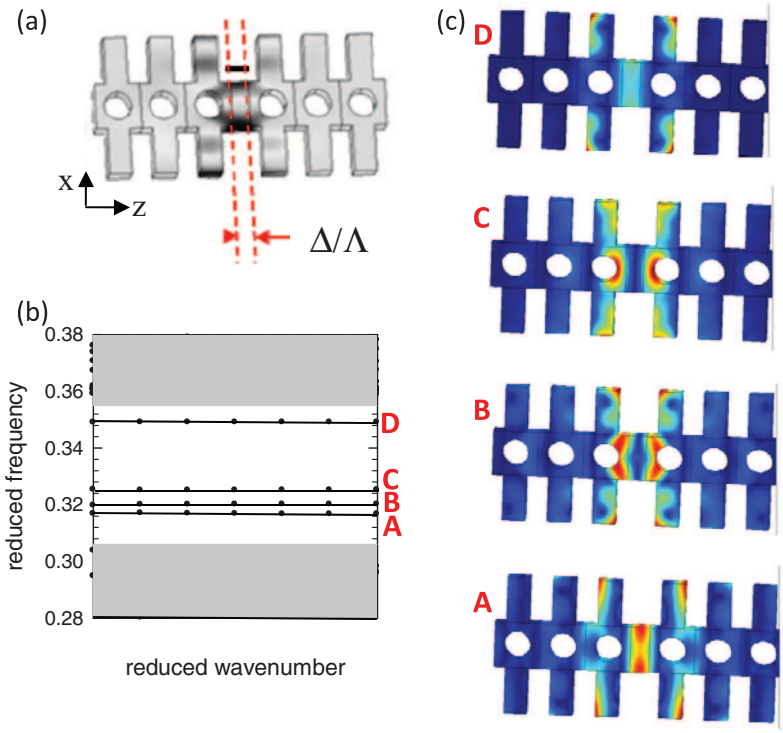

FIG. 5. (a) Geometry of the cavity defined by the length Δ. (b) Phononic dispersion diagram along the ΓX direction of the strip waveguide, for a cavity of length $\Delta/\Lambda=0.4$. (c) Modulus of the displacement field calculated at the points A, B, C, and D of the dispersion curves.

phonons and photons in a cavity (Fig. 5(a)) inserted in the strip waveguide. The cavity is created by simply changing the distance between two neighboring unit cells along the z direction, as depicted in figure 5(a). The width of the cavity is characterized by the elongation parameter Δ, i.e. $\Delta=0$ when the crystal is perfect.

We calculate the phononic band structure by FEM using a super-cell constituted of the cavity surrounded by three periods of the phoxonic crystal strip on each side (Fig.5(a)). The separation between two neighboring cavities is sufficient to avoid interaction between them. The dispersion diagram is shown in Fig. 5(b) for a cavity of length $\Delta/\Lambda=0.4$. The white area representing the band gap is delimited by the propagating bands (grey areas) of the perfectly periodic structure. The

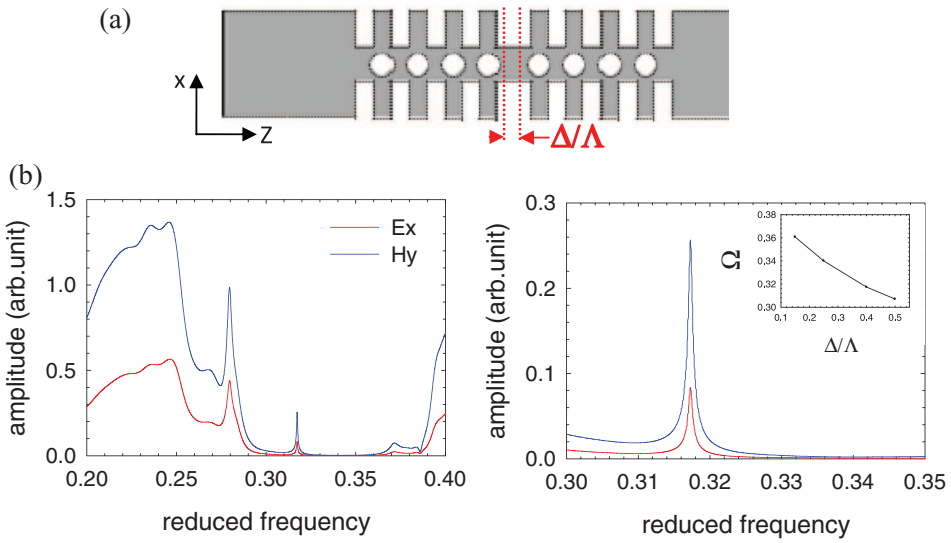

FIG. 6. (a) Schematic view of the (x,z) section of the structure used for the 3D-FDTD calculation of transmission, with $\Delta/\Lambda=0.4$. (b) Left: Transmission coefficients for the electric and magnetic fields displaying a resonant peak inside the gap. Right: Magnification of the resonant peak. The inset shows the evolution of the peak frequency as a function of Δ.

insertion of a defect cavity introduces new branches inside the band gap corresponding to modes confined inside the cavity. These branches move downwards and their number increases as the size of the cavity increases.

The flatness of the branches is a signature of their confinement inside the cavity. To support this statement, we display in Fig. 5(c) the modulus of the displacement field for the modes labeled A, B, C and D in Fig. 5(b). Depending on the considered mode, the displacement field is essentially localized inside the defect cavity and inside the first stubs surrounding the cavity.

On the photonic side, dispersion diagrams obtained with the super-cell method are not easily interpreted. This is due to the many folding of the bands in the reduced Brillouin zone that is associated to the super-cell, giving rise to a large number of branches above the light line. In this case, it is more efficient to directly calculate the transmission coefficient when an incident wave is launched towards the strip and to explore the possibility of a wave being confined inside the cavity. This calculation is performed with the help of a homemade three-dimensional finite difference time domain (3D-FDTD) code. The model is composed of a 3D-box made up of the silicon strip waveguide embedded in air with perfect matching layers (PML) conditions applied at all boundaries. The structure (figure 6(a)) is constituted by (i) an incoming straight waveguide where light is injected, (ii) the periodic waveguide composed of eight unit cells and the central cavity, and (iii) an outgoing straight waveguide where the output signal is detected. Space is discretized in both three directions using a mesh interval equal to $\Lambda/20$. The equations of motion are solved with a time integration $\Delta t = \Delta x/(4c)$, where c is the velocity of light in vacuum, and a number of time step equal to 2^{22}, which is the necessary time for a good convergence of the numerical calculation.

The injected pulse is generated at the left side of the 3D-box by a current source appropriate to create the optical wave with the desired symmetry, which in our case should be respectively odd and even with respect to the symmetry planes Π' and Π. The transmitted signal, probed at the end of the right part of the strip waveguide, is recorded as a function of time and finally Fourier transformed to obtain the transmitted amplitude of the fields versus reduced frequency.

Figure 6(b) shows the amplitude of the transmitted electric and magnetic fields. In the presence of the cavity, a sharp peak appears inside the band gap at the reduced frequency 0.3172. This peak is magnified in the right part of figure 6(b). In the inset of the figure, we show the evolution of the frequency of the peak as a function of the length Δ/Λ of the cavity. This frequency decreases by increasing Δ, so the position of the resonant mode can be tuned inside the gap.

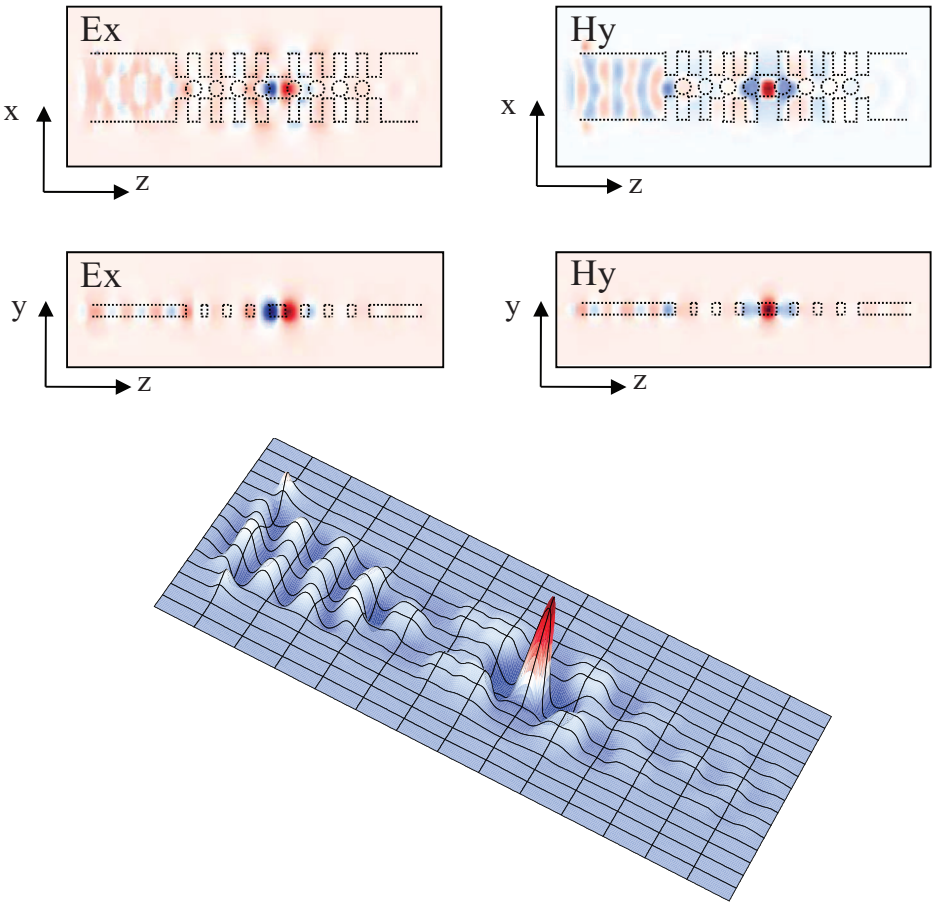

FIG. 7. (a) Maps of the electric and magnetic fields in the strip waveguide structure containing a cavity with length $\Delta/\Lambda=0.4$ at the monochromatic frequency 0.3172. (b) 3D map of the magnetic field.

To give a better view of the confinement of the resonant mode, we show in Fig.7 the maps of the electric and magnetic fields for a monochromatic excitation at the reduced frequency of the peak (0.3172).

As a conclusion, the introduction of a cavity of length $\Delta/\Lambda=0.4$ in the strip waveguide allows us to obtain simultaneous confinement of both acoustic and optical waves inside the cavity. A look at the maps of the confined modes shows that the most significant overlap between both waves, which is a necessary condition to enhance their interaction, is achieved with the acoustic cavity mode named (A) in figure 5(c).

It is worthwhile noticing that in the above calculations the geometrical parameters were defined in comparison with the period Λ of the structure taken as the unit of length. Therefore, the phenomena described in this paper can be produced in different frequency ranges depending on the actual value of Λ. If the working optical frequency is chosen to be at the telecommunication wavelength of 1550 nm, then the geometrical parameters become $\Lambda=500$ nm, $w_e=1500$ nm, $w_i=250$ nm, $h=220$ nm, $r=150$ nm and $\Delta=200$ nm. These parameters make the periodic strip waveguide technologically feasible. In this case, the acoustic mode (A) of Fig. 5(c) has a resonance frequency of 3.7 GHz.

V. CONCLUSION

In this work, we have investigated theoretically a periodical silicon nanowire made up of a straight waveguide combined with symmetric stubs grafted on each side and circular holes drilled in the middle. Appropriate choices of the geometrical parameters have allowed us to obtain a complete

phononic gap together with a photonic gap of a given polarization and symmetry. We have shown that stubs and holes are respectively favorable for creating a phononic and a photonic band gap. We have then investigated the possibility of confining modes inside a defect cavity inserted in the phoxonic strip waveguide. Such a cavity can simultaneously confine phonons and photons, providing with an overlap of their fields which can enhance their interaction. Finally, we have discussed actual values of the geometrical parameters, compatible with technological fabrication constraints, in order to find the photonic cavity mode in the range of telecommunication wavelengths, with the acoustic frequencies falling in the gigahertz range.

ACKNOWLEDGMENTS

This work was supported by the European Commission Seventh Framework Programs (FP7) under the FET-Open project TAILPHOX N° 233883.

[1] M. S. Kushwaha, P. Halevi, L. Dobrzynski and B. Djafari-Rouhani, Phys. Rev. Lett. **71**, 2022-2025 (1993).
[2] M. M. Sigalas and E. N. Economou, Solid State Commun. **86**, 141 (1993).
[3] E. Yablonovitch, J. Opt. Soc. Am. B **10**, 283 (1993).
[4] T. F. Krauss, R. M. De la Rue, and S. Brandt, Nature **383**, 699 (1996).
[5] Y. Pennec, J. O. Vasseur, B. Djafari-Rouhani, L. Dobrzyński, and P. A. Deymier, Surface Science Reports **65**, 229 (2010).
[6] S. Fan, P. Villeneuve, J. Joannopoulos, and H. Haus, Opt. Express **3**, 4 (1998).
[7] S. Shi, C. Chen, and D. W. Prather, J. Opt. Soc. Am. A **21**, 1769 (2004).
[8] S. G. Johnson, S. Fan, P. R. Villeneuve, J. D. Joannopoulos, and L. A. Kolodziejski, Phys. Rev. B **60**, 5751 (1999).
[9] A. Khelif, B. Aoubiza, S. Mohammadi, A. Adibi, and V. Laude, Phys. Rev. E **74**, 046610 (2006).
[10] C. Charles, B. Bonello, and F. Gannot, Ultrasonics **44**, 1209(E) (2006).
[11] J. O. Vasseur, P. A. Deymier, B. Djafari-Rouhani, Y. Pennec and A. C. Hladky-Hennion, Phys. Rev. B **77**, 085415 (2008).
[12] Y. Pennec, B. Djafari-Rouhani, H. Larabi, J. O. Vasseur and A. C. Hladky-Hennion, Phys. Rev. B **78**, 104105 (2008).
[13] T. T. Wu, Z. G. Huang, T. C. Tsai, and T. C. Wu, Appl. Phys. Lett. **93**, 111902 (2008).
[14] J. S. Foresi, P. R. Villeneuve, J. Ferrera, E. R. Thoen, G. Steinmeyer, S. Fan, J. D. Joannopoulos, L. C. Kimerling, H. I. Smith and E. P. Ippen, Nature **390**, 143, 1997.
[15] A. R. Md Zain, N. P. Johnson, M. Sorel, and R. M. De La Rue, Opt. Express **16**, 12084 (2008).
[16] Y. Pennec, B. Djafari-Rouhani, A. Akjouj, J. O. Vasseur, L. Dobrzynski, J. P. Vilcot, M. Beaugeois, M. Bouazaoui, R. Fikri, and J. P. Vigneron, Appl. Phys. Lett. **89**, 101113 (2006).
[17] F. C. Hsu, C. I. Lee, J. C. Hsu, T. C. Huang, C. H. Wang, and P. Chang, Appl. Phys. Lett. **96**, 051902 (2010).
[18] M. Maldovan and E. L. Thomas, Appl. Phys. Lett. **88**, 251907 (2006).
[19] M. Maldovan and E. L. Thomas, Appl. Phys. B. **83**, 595 (2006).
[20] S. Sadat-Saleh, S. Benchabane, F. I. Baida, M. P. Bernal and V. Laude, J. Appl. Phys. **106**, 074912 (2009).
[21] D. Bria, M. B. Assouar, M. Oudich, Y. Pennec, J. Vasseur, and B. Djafari-Rouhani, J. Appl. Phys. **109**, 014507 (2011).
[22] S. Mohammadi, A. A. Eftekhar, A. Khelif, and A. Adibi, Opt. Express **18**, 9164 (2010).
[23] Y. Pennec, B. Djafari-Rouhani, E. H. El Boudouti, C. Li, Y. El Hassouani, J. O. Vasseur, N. Papanikolaou, S. Benchabane, V. Laude, and A. Martinez, Opt. Express **18**, 14301 (2010).
[24] Y. El Hassouani, C. Li, Y. Pennec, E. H. El Boudouti, H. Larabi, A. Akjouj, O. Bou Matar, V. Laude, N. Papanikolaou, A. Martinez, and B. Djafari Rouhani, Phys. Rev. B, **82**, 155405 (2010).
[25] A. H. Safavi-Naeini, O. Painter, Opt. Express **18**, 14926 (2010).
[26] V. Laude, J. C. Beugnot, S. Benchabane, Y. Pennec, B. Djafari-Rouhani, N. Papanikolaou, J. M. Escalante, A. Martinez, Opt. Express **19**, 9690 (2011).
[27] Y. Pennec, B. Djafari Rouhani, E. H. El Boudouti, C. Li, Y. El Hassouani, J. O. Vasseur, N. Papanikolaou, S. Benchabane, V. Laude, and A. Martinez, Chinese Journal of Phys. **49**, 100.
[28] E. Gavartin, R. Braive, I. Sagnes, O. Arcizet, A. Beveratos, T. J. Kippenberg, Phys. Rev. Lett. **106**, 203902 (2011).
[29] D. A. Fuhrmann, S. M. Thon, H. Kim, D. Bouwmeester, P. M. Petroff, A. Wixforth, and H. J. Krenner, Nature Photonics **5**, 605 (2011).
[30] M. Eichenfield, J. Chan, R. M. Camacho, K. J. Vahala, and O. Painter, Nature **462**, 78 (2009).
[31] M. Eichenfield, J. Chan, A. H. Safavi-Naeini, K. J. Vahala, O. Painter, Opt. Express **17**, 20078 (2009).